Published in final edited form as:
NMR Biomed. 2012 January ; 25(1): 169–176. doi:10.1002/nbm.1732.

CHARACTERIZATION OF SKIN ABNORMALITIES IN A MOUSE MODEL OF OSTEOGENESIS IMPERFECTA USING HIGH RESOLUTION MAGNETIC RESONANCE IMAGING AND FOURIER TRANSFORM INFRARED IMAGING SPECTROSCOPY

Holly C. Canuto[1,#], **Kenneth W. Fishbein**[1], **Alice Huang**[2], **Stephen B. Doty**[2], **Ron A. Herbert**[3], **John Peckham**[3], **Nancy Pleshko**[2,4], and **Richard G. Spencer**[1]

[1]Magnetic Resonance Imaging and Spectroscopy Section, NIH/National Institute on Aging, Intramural Research Program, GRC 4D-08 5600 Nathan Shock Drive, Baltimore, MD 21224

[2]The Hospital for Special Surgery, 535 E. 70th St., New York, NY 10021

[3]National Institute of Environmental Health Sciences, National Institutes of Health, Research Triangle Park, NC 27709

[4]Dept. of Mechanical Engineering, Temple University, Philadelphia, PA

INTRODUCTION

Osteogenesis imperfecta (OI) is a heritable disorder of connective tissue characterized by bone fragility, caused primarily by mutations in the genes that encode for the pro-α1 and pro-α2 chains of type I collagen. The mildest form of OI, Type I(1), results in relatively few fractures and a normal life expectancy, while Type II, the most severe form, is characterized by severe multiple intrauterine fractures and perinatal mortality. Types III and IV show moderate-to-severe symptoms. At the molecular level, these phenotypes are characterized by the region and extent of mutation (2–4). Additional OI phenotypes have more recently been identified (5).

Skin manifestations of OI have been investigated previously (6–9). Decreased skin collagen content was demonstrated in transgenic mouse models of OI types I and II (10,11) as well as in human skin (9), while significant decreases in elasticity, distensibility, and hysteresis were found in patients with mild and moderate-to-severe OI (12). Early histochemical and electron microscopical studies showed thinning of the dermal layers in a sample of skin from a 40 week-old human (8) and diffuse and unstructured collagen packing in severe OI (9). While these studies evaluated skin characteristics in OI, they did not undertake precise delineation and characterization of individual skin layers. In severe OI, diagnosis is somewhat straightforward, based on the clinical picture of multiple fractures and deformities. However, the diagnosis of more mild phenotypes is significantly more difficult, involving biochemical assessment of the collagen produced from biopsy-derived dermal fibroblasts (13–15). A rapid non-invasive diagnostic approach would be of significant value in this setting, permitting implementation of appropriate lifestyle modifications (16) and, potentially, initiation of antiresorptive therapy (17). Further, since unexplained fractures in

Address for correspondence: Richard G. Spencer, Magnetic Resonance Imaging and Spectroscopy Section, NIH/National Institute on Aging, Intramural Research Program, GRC 4D-08, 5600 Nathan Shock Drive, Baltimore, MD 21224, Tel: 410-558-8226, FAX: 410-558-8318, spencer@helix.nih.gov.
[#]Present affiliation: University of Cambridge and Cancer Research UK, Department of Biochemistry, Sanger Building, 80 Tennis Court Road, Cambridge, CB2 1GA, UK.

infants are characteristic of both OI and of deliberate injury (13,18–20), a rapid diagnostic test would be of value in assessing the household environment of infants presenting with fracture. These facts motivate a study of skin phenotype in OI in an appropriate pre-clinical model.

An established murine model of OI is the *oim* mouse, a naturally occurring recessive mutation (21). Mice homozygous for this mutation (*oim/oim*) are deficient in pro-α2(I) collagen, and their type I collagen is predominantly a pro-α1(I) homotrimer. The biochemical and phenotypic characteristics of this mouse are similar to those seen in patients with type III OI, and include osteopenia, skeletal fractures, and deformities (22). The phenotypic features of the heterozygote, the *oim/+* mouse, include mild bone fragility and decreased collagen content, similar to features characteristic of type I OI (23,24).

The clinical and experimental use of magnetic resonance imaging (MRI) to provide highly detailed anatomic and biophysical characterization of soft tissues, including cartilage and skin, is well-established. Application to skin has been comparatively limited, although increases in magnetic field and gradient strength as well as improvements in coil design have permitted increased investigation of skin characteristics in vivo and ex vivo (25–34). MRI parameters such as transverse relaxation time (T2) and magnetization transfer (MT) rate or ratio are sensitive to collagen in the layers of skin (27) as well as in cartilage (35–41) in normal and pathological samples. However, the effects of OI-associated collagen I mutations on skin have not been evaluated by MRI.

We hypothesized that skin abnormalities would be seen in the oim mouse, consistent with the known collagen mutation, and that these abnormalities would be detectible by non-invasive MRI analysis of tissue morphology and biophysical characteristics. We further hypothesized that MRI studies would have the capability to differentiate among OI homozygous (*oim/oim*), OI heterozygous (*oim/+*), and wild type (+/+) mouse skin. Results were correlated with histologic studies, and with Fourier transform infrared imaging spectroscopy (FT-IRIS) to establish molecular-level characteristics of the tissue. FT-IRIS in an extension of conventional infrared spectroscopy in which an FTIR spectrometer is coupled to an optical microscope equipped with an array detector, thereby permitting evaluation of the relative amount and distribution of the molecular components of connective tissue. Use of these complementary techniques resulted in significant insight into the differences observed in the MRI data obtained from the three genotypes.

MATERIALS AND METHODS

Animals

Tissue samples were obtained from genotype-verified B6C3 wild type (+/+), heterozygous (*oim/+*), and homozygous (*oim/oim*) mice through an IACUC-approved protocol at Hospital for Special Surgery. Animals were sacrificed at 11 weeks of age at which time skin samples (ca. 15 mm long × 10 mm wide) were taken from the back (+/+, n = 6 male and 6 female; *oim/+*, n = 3 male and 1 female, and *oim/oim*, n = 6 male and 6 female).

Magnetic Resonance Imaging

Skin samples were stretched onto opposite sides of a planar wooden sample holder with the exterior skin surfaces facing outward and immersed in a protease inhibitor solution in a 15 mm NMR tube. Imaging was carried out using a 9.4 Tesla 105 mm vertical bore magnet (Magnex Scientific, Abingdon, UK) interfaced to a Bruker DMX 400 NMR spectrometer, a Micro2.5 microimaging probe equipped with 1000 mT/m three-axis actively shielded gradients, and a 15 mm birdcage resonator (Bruker Biospin MRI, Ettlingen, Germany).

Images were acquired with a 2D spin-echo sequence, with field of view = 0.75 cm × 1.5 cm and matrix size of 512 × 256, resulting in an in-plane resolution of 13 μm (read) × 58 μm (phase encode). The read direction was perpendicular to the skin surface, providing maximum resolution with respect to depth from the surface of the skin. Slice thickness was 1 mm. A minimum echo time TE=12 ms and TR=4s was used for all experiments. T2 maps were obtained using a train of six equally spaced echoes. Magnetization transfer experiments were carried out with $B_{1,sat}$= 12 μT, saturation offset = +15 ppm from water, and saturation pulse length ranging from 1 ms to 4.6 ms in 12 increments. The apparent MT exchange rate, k_m, was derived from measurement of observed signal intensity as a function of off-resonance saturation time. In selected experiments, fat suppression, a spectroscopic technique used to identify and suppress the presence of fat signals, was applied in order to identify fatty layers within each skin sample.

Histology

After MRI studies were completed on each sample, tissue was fixed in 80% ethanol and embedded in paraffin. Histology was performed on 5 μm-thick sections, with hematoxylin and eosin (HE) staining used to visualize general tissue morphology, Masson's trichrome staining used to delineate collagen-rich regions with relief provided by cytoplasm and nuclei, and the Luna stain used for identifying elastin fibers and mast cells. Elastin fibers and mast cells stain purple with Luna, nuclei stain black, and the background stains yellow.

Fourier Transform Infrared Imaging Spectroscopy (FT-IRIS)

After paraffin embedding as described above, 6-micron thick sections were placed onto BaF_2 windows. Spectra were acquired with a Spectrum SpotLight 300 FTIR imaging system (Perkin-Elmer, UK), consisting of an FTIR spectrometer coupled to an optical microscope and a 2 × 8 array of linear infrared detectors, allowing rectangular samples up to several millimeters in length to be imaged. The spatial resolution of the measurements was 25 microns, with a spectral resolution of 8 cm$^{\#x02212;1}$. Spectra were also acquired from pure melanin powder to identify spectral features unique to melanin. Data were analyzed utilizing ISys software v4.0 (Spectral Dimensions, Olney, MD).

The number of spectra analyzed for each sample ranged from ~ 800 to 1800, depending upon the size of the skin sample. The 1652 cm$^{\#x02212;1}$ amide I absorbance band was used to map the distribution of protein throughout the specimen (42), while the 1716 cm$^{\#x02212;1}$ absorbance band was used to map the distribution of melanin. Images were spatially masked to include only the dermal layer for analysis of collagen molecular properties. The ratio of the integrated area under the 1338 wavenumber peak (1356–1324 cm$^{\#x02212;1}$) to the area under the amide II peak (1588–1488 cm$^{\#x02212;1}$) was used as an indicator of collagen integrity (43). The ratio of the peak heights at 1660 cm$^{\#x02212;1}$ and 1690 cm$^{\#x02212;1}$ was taken as a qualitative indicator of the ratio of mature and immature collagen crosslinks (44).

Statistical Analysis

Data are shown as mean ± standard error of the mean. Quantitative data from MRI and FT-IRIS analyses were analyzed by one-way analysis of variance (ANOVA) followed by the Tukey post-hoc test. Differences were considered statistically significant at the $p < 0.05$ level.

RESULTS

Histology

The skin of the +/+ mice was histologically normal, with Luna (Fig. 1a) and Masson's trichrome (Fig. 1b) staining clearly delineating the epidermis (layer l), the collagen-rich

papillary and reticular layers of the dermis (layer ll), and the hypodermal fat (layer lV). The dermal layer in the skin of homozygous mice (Luna, Fig. 1c; Masson's trichrome, Fig. 1d) were markedly different from the corresponding layers in the +/+ animals. A reduction by approximately 60% in the dermal thickness layer ll was observed, but due to the presence of a third layer immediately below this layer, labeled as layer lll, the overall skin thickness was unchanged. In addition, there were large numbers of prominent, actively growing hair follicles in the upper dermal layer (layer ll) as well as in the extended lower dermal layer (layer lll). The majority of these follicles were in the anagen stage of hair growth with large, heavily pigmented, melanin-rich hair bulbs. The hair shafts had thick root sheaths, while sebaceous glands were smaller and less conspicuous. Masson's trichrome stain (Fig. 1b and 1d) demonstrated a markedly reduced region of collagen-rich tissue in the *oim/oim* animals, confirming that the basic histopathologic alteration was loss of dermal collagen, whereas the Luna stain (Fig. 1a and 1c) indicated an absence of elastin fibres in the lower dermal layer (layer lll). Heterozygous mice were variably affected; only one of the four mice examined had a loss in dermal thickness, of approximately 40%, as determined by both Masson's trichrome and the Luna stain (data not shown).

MRI Analysis

Anatomic Analysis—Typical T2-weighted MR images showed a clear demarcation of individual skin layers (Fig. 2). Fat suppression (labeled with "b" in Figure) caused the hypodermal fat layer to be darkened, allowing it to be unambiguously identified and used as a reference for the other skin layers. The most superficial layer, labeled as layer I, corresponds to the epidermis in all genotypes. In the +/+ samples, layer ll consists of the papillary (lla) and reticular dermis (llb), similar to what is seen in the accompanying histology (Figure 3). Layer lV consists largely of fat.

Differences in the thickness and contrast of these skin layers were evident upon comparison of the homozygous to wildtype control images. The clear separation of the dermal layer into an upper (layer lla) and lower layer (layer llb) was seen in all homozygous mice, but was variable in the *oim/+* animals (Fig. 2). The additional layer, lll, observed in the *oim/oim* mice histology, was also present in the MR images. Thus, an approximate correspondence can be established between the layers observed in MRI and in histology (Fig. 3). Horizontal banding seen occurring throughout layer III in the *oim/oim* mouse is consistent with inhomogeneous hydration in this skin layer. The average thickness of the skin layers as visualized by MRI is shown in Fig. 4a. The most striking finding is that the upper dermal layer (layer ll) comprises only 28% and 36% of the skin thickness in homozygous (*oim/oim*) and heterozygous (*oim/+*) mice, respectively, compared to 72% in wild type mice. This is attributable to the presence of the additional layer lll in the oim genotypes. The epidermal thickness (layer l) was not significantly different among the three genotypes. The the hypodermal fat layer (layer lV) did not remain fully intact upon dissection, and therefore thickness was not evaluated.

Biophysical Characteristics—Overall, the highest T2 values were seen in the hypodermal fat layer lV (Fig. 4b). In the lower dermal layer lll of the *oim/oim* skin samples, the T2 values were comparable to those in the corresponding hypodermal fat layer lV. T2 values for the heterozygote specimens were significantly higher ($p < 0.05$) than for the *oim/oim* and +/+ tissues in the collagen-rich dermis, layer ll. MT rate ($k_m/s^{\#x02212;1}$) values for the epidermal, dermal and hypodermal fat layers were comparable among genotypes. Similar MT rates were found between the lower dermal *oim/oim* layer lll and the hypodermal fat layer lV. A significantly higher MT rate was found between layer ll (combined papillary and reticular dermis) and layer lll in *oim/oim* and in *oim/+* tissues.

FT-IRIS Analysis—The infrared spectrum obtained from the dermal layer in a wildtype mouse (Fig. 5a) is dominated by the broad amide I band typical of collagen, and also contains features that arise from other collagen vibrations, including the 1338 $cm^{\#x02212;1}$ sidechain rotation absorbance, and from the paraffin embedding medium. The spectrum of pure melanin powder (Fig. 5b) has an identifying feature at 1716 $cm^{\#x02212;1}$, which was used to map the distribution of melanin in the dermal layers of the skin. The protein content, mapped by the amide I band, was greater in the dermal than in the fatty layer for all genotypes (Fig. 6), reflecting the collagen-rich upper dermal layer. There was a strong correspondence between the distribution of the dark, spotted regions in the dermal layer of the HE stained sections and the distribution and concentration of melanin as determined by FT-IRIS, confirming their chemical composition. The collagen integrity index was found to be significantly lower in the *oim/oim* as compared to both the +/+ and *oim/+* tissues (Fig. 7a). Finally, a small but significantly lower mature to immature crosslinks ratio was observed in the *oim/oim* and *+/oim* tissues compared to the +/+ tissues (Fig. 7b).

DISCUSSION

Clinical manifestations of OI typically present through bone pathology, although phenotypic alterations involving other collagen I containing tissues, such as sclerae, dentin, and ligaments are also present (8,9,13,45). Less well-investigated are the cutaneous manifestations of the underlying collagen I defect, which may be particularly amenable to evaluation by MRI.

Impairment of collagen fibril association is characteristic of connective tissue disorders and results in a weaker and less densely packed collagen network (7,46). In this study, we sought to examine manifestations of this and potential loss of collagen in the skin in a mouse model of OI, using histology to provide a qualitative assessment of morphological changes and collagen content, MRI to delineate large-scale structural features and biophysical characteristics, and FT-IRIS to examine molecular features of the matrix.

The MRI parameters studied in the present work, the spin-spin relaxation time T2, and the MT rate, have been widely applied to the study of soft tissue. MT can also be evaluated through the MT ratio, which represents an MR signal intensity ratio in the presence and absence of radio-frequency power applied to immobile macromolecules. This ratio provides an indication of the net transfer of magnetization, through either chemical exchange or dipole-dipole interactions, from immobile protons to observed protons in bulk water. The transfer rate itself, k_m, can also be quantified and, unlike MT, does not depend explicitly upon longitudinal relaxation, that is, upon T1. Therefore, in our analysis, we have presented results for k_m rather than for MT.

T2 and k_m are sensitive to a number of biophysical tissue characteristics. In cartilage, increased MT ratio and k_m have been generally associated with increased macromolecular, and in particular collagen, content. In a study of k_m as a function of collagen concentration in gels, values in the range of 1 to 2 $sec^{\#x02212;1}$ were obtained for collagen concentrations above 5% w/v, with k_m clearly increasing as a function of concentration (47). These values are similar to those obtained in our study; this is consistent with an interpretation in which collagen concentration is the dominant determinant of the MT phenomenon, even in a complex tissue such as skin. Indeed, comparable values for k_m were also found in the very different environment of developing engineered cartilage tissue (48). In addition, while k_m as a function of collagen concentration was not directly presented, there was a clear increase with concentration in a related parameter, $MTR=k_mT1_{,sat}$, with the latter quantity being the T1 value for free water obtained in the presence of the radio-frequency power applied to immobile macromolecules as described above. Finally, although a dependence of

magnetization transfer on collagen cross-linking has been clearly established (49,50), and a cross-linking defect has been long-recognized in human OI (51), we did not detect a difference in k_m among comparable layers in the skin of the +/+, *oim/+*, and *oim/oim* mice. However, although the extent of collagen cross linking was not measured directly in this study, the ratio of mature to immature cross links, as estimated by the collagen crosslink parameter from the IR analysis, was significantly lower in the *oim/+* and *oim/oim* mice as compared to controls.

In skin, the degree of magnetization transfer has been shown to be highest in the epidermal and papillary dermal layers and lowest in the reticular dermis (52,53), consistent with our observations. Thus far, however, the effects of the OI-associated collagen I mutation in the dermis have not been evaluated by MRI. In fact, while MR studies are sensitive to both collagen I and II (36,38), there has been negligible success in discriminating between them with MRI, although one study reported some difference in MT rate between collagen type I and II gels of equal macromolecular concentration (36). However, the focus of the present study was not to distinguish between collagen types, but rather to exploit the established dependencies of MRI parameters on collagen content.

Relationships between tissue hydration and T2 relaxation rates have been well-established in cartilage and isolated collagen fibrils (48,54,55), with the greater water mobility associated with increased hydration being reflected in larger T2 values. T2 is also sensitive to collagen content (48,56) and is therefore often used to evaluate cartilage degeneration. Similarly, T2 measurements have been taken as reflecting bound and free water content in skin layers (31). Like k_m, T2 is also dependent upon collagen crosslinking; decreased T2 is seen with greater degrees of crosslinking (50). As was also the case for k_m, we did not observe a T2 difference between the corresponding layers in +/+ and *oim/oim* skin, indicating that the IR parameters are more sensitive to this molecular feature.

Finally, we note that the T2 parameter itself, representing the conventional monoexponential time constant for spin-spin relaxation, is itself an approximation to what is more likely multiexponetial relaxation arising from multiple tissue compartments in each skin layer. In a study of hydrated collagen II (55), two components with relaxation times that depended upon the degree of collagen hydration were detected. Values were in the range of 5 ms and 100–200 ms, respectively. The more rapidly relaxing component was the more abundant of the two, so that a monoexponential fit to the relaxation data would be expected to fall closer to that shorter value, as was observed in the present work. Somewhat different values have been obtained using a different measurement technique (57), but confirmed the presence of multiple T2 components representing compartmented water. Of course, comparison between results obtained on hydrated collagen and on intact skin can be interpreted in qualitative terms only. Multiexponential T2 relaxation has also been observed in native and degraded cartilage, which, like skin, has a large collagen content (58). Multiexponential T2 analysis has not yet been carried out in skin, to our knowledge, but such experiments are likely to yield insight into the biophysical microstructure and interactions between compartments of that tissue (49). Implementation, however, would be complicated by the need for highly spatially resolved measurements.

The most striking features of the histologic data are the changes in layer thickness and the introduction of a new layer, layer lll, located beneath the usual dermal layer, layer ll, in the *oim/oim* mouse. The marked thinning of the dermis, the most collagen-rich of the skin layers, is consistent with the underlying collagen defect of OI. This thinning was seen in skin samples from the homozygous *oim/oim* mice and, to a lesser extent, in heterozygous *oim/+* mice; this represents an intermediate phenotype in the heterozygote, as has also been reported in other tissues (24). Masson's trichrome staining was consistent with a less well-

organized collagen network in the upper dermal layer (layer ll) in the homozygotes as compared to the wildtype, accompanied by thinning of this layer. Finally, the marked increase in the number of melanin-rich hair bulbs in the anagen stage of growth seen in the *oim/oim* samples is consistent with a more hydrophilic environment due to decreased collagen content and impaired packing (59).

In this study high-resolution MRI permitted the visualization of the epidermal, dermal and hypodermal fat layers of the skin. The physical-chemical basis of MRI contrast differs from that of histologic staining, so that it is not to be expected that the morphology of the delineated layers will be identical between the two modalities. However, MRI findings largely recapitulated those from histology. The thinning of the upper dermal layer in the homozygotes was well visualized, as was the presence of the thicker inferior dermal layer, as compared to the wildtype. These features were also seen, though less consistently, in the heterozygous mice. The possibility that the inferior dermal layer might be an extension of the hypodermal fat layer (layer lV) was ruled out by the application of spectroscopic fat suppression, which attenuated the signal from the fat layer, as expected, but not from the inferior dermal layer.

Transverse relaxation times in the range of 10–23 ms have been reported in the dermis (29), consistent with the values reported here. The larger value of T2 seen in the upper dermal (ll) layer in the homo- and heterozygous OI mice, as compared to the same layer in the wild type, is consistent with increased hydration in this collagen-rich zone, reflecting the fact that T2 increases with hydration. In the present case, this may be due to lower collagen concentration or impaired lateral packing resulting from the absence of the α2(I) chain in the *oim/oim* mice, and the presence of both homotrimeric and heterotrimeric collagen I fibrils in the *oim/+* mice (60). Thus, the noninvasive MRI data is consistent with known characteristics of these genotypes. The largest value of T2 for layer ll was seen in the *oim/+* skin; this is consistent with the finding of the largest lateral distance between collagen monomers in *oim/+* as compared to +/+ and *oim/oim* mice (60). The reason for the comparable finding in layer lV, the fat layer, is less clear.

The MT rate in layer lll was 40–50% smaller than in layer ll in homozygous (*oim/oim*) and heterozygous (*oim/+*) mouse skin, consistent with a lower collagen content in layer lll. In contrast, MT rate was similar among genotypes within each skin layer.

FT-IRIS clearly demonstrated distinct dermal layers and their most prominent macromolecular characteristics. The collagen integrity parameter as used here was developed as a measure of collagen helical instability in cartilage (43) and has not been validated as a marker of skin collagen characteristics. Nevertheless, as a marker of a collagen-specific, rather than a tissue-specific, feature, it is plausible that its interpretation with respect to skin collagen would be similar. This parameter was found to be lowest in the *oim/oim* skin, consistent with decreased collagen quality in that phenotype.

The FTIR collagen crosslink parameter was developed to probe the ratio of immature to mature collagen crosslinks in bone (44). Biochemical studies have demonstrated a significant reduction of stabilizing intermolecular crosslinks in bone in the *oim/oim* mouse (42). Our finding of a decrease in this parameter in the skin of the *oim/oim* and *oim/+* mice as compared to the wildtype is consistent with previous findings (9). FTIR and MRI have been used previously in a complementary fashion to assess collagen-containing tissues (61). This combined approach builds on previous work exploiting proteoglycan-sensitive MRI (62) and FT-IRIS (63) methods for tissue analysis. In the present study, the results of combined MRI and FT-IRIS analyses are consistent with a decrease in collagen content as

well as potential alteration in the integrity of the collagen framework. These findings are consistent with the skin fragility and reduced elasticity seen in OI(12,64).

Formation of the stable collagen triple helix structure within the skin of the homozygous (*oim/oim*) mice is inihibited by the complete absence of the hydrophobic proα2(I) chain (21,65). This may lead to a particularly hydrophilic environment, as manifest in the observation of increased T2 in these mice. These findings are further consistent with the histologic findings of hair follicles in the anagen stage of growth within the lower dermal layer of homozygous mice, since this growth stage is favored in a hydrophilic environment (59), as would be consistent with decreased collagen content. Studies of the conditions promoting the follicle anagen stage have also indicated the presence of a rapid rate of collagen framework remodeling, attenuating crosslinking in collagen fibrils (59). This is consistent with the present FT-IRIS data indicating a smaller ratio of mature to immature collagen crosslinks in the dermis of OI mice.

In summary, MRI analysis of the skin of mouse models of OI demonstrated marked differences compared to control animals, and are consistent with histologic and FT-IRIS analysis. MRI was sensitive to collagen-related alterations in the skin of OI mice as evidenced by the increased T2 and by the differences within layers in the MT parameter. We conclude that MRI and FT-IRIS represent powerful complementary techniques for the assessment of skin abnormalities in animal models of disease.

Acknowledgments

This research was supported by the Intramural Research Program of the NIH, National Institute on Aging and NIH grant AR48337 (NP).

Nonstandard Abbreviations

MRI	Magnetic Resonance Imaging
FT-IRIS	Fourier Transform Infrared Imaging Spectroscopy
OI	Osteogenesis Imperfecta

REFERENCES

1. Sillence DO, Senn A, Danks DM. Genetic heterogeneity in osteogenesis imperfecta. J Med Genet. 1979; 16(2):101–116. [PubMed: 458828]
2. Dalgleish R. The human type I collagen mutation database. Nucleic Acids Res. 1997; 25(1):181–187. [PubMed: 9016532]
3. Dalgleish R. The Human Collagen Mutation Database 1998. Nucleic Acids Res. 1998; 26(1):253–255. [PubMed: 9399846]
4. Ward LM, Lalic L, Roughley PJ, Glorieux FH. Thirty-three novel COL1A1 and COL1A2 mutations in patients with osteogenesis imperfecta types I–IV. Hum Mutat. 2001; 17(5):434. [PubMed: 11317364]
5. Cheung MS, Glorieux FH. Osteogenesis Imperfecta: update on presentation and management. Rev Endocr Metab Disord. 2008; 9(2):153–160. [PubMed: 18404382]
6. Holbrook KA, Byers PH, Pinnell SR. The structure and function of dermal connective tissue in normal individuals and patients with inherited connective tissue disorders. Scan Electron Microsc. 1982; (Pt 4):1731–1744. [PubMed: 6892170]
7. Holbrook KA, Byers PH. Skin is a window on heritable disorders of connective tissue. Am J Med Genet. 1989; 34(1):105–121. [PubMed: 2683775]

8. Haebara H, Yamasaki Y, Kyogoku M. An autopsy case of Osteogenesis Imperfecta Congenita - Histochemical and Electron Microscopical studies. Acta Path Jap. 1969; 19(3):377–394. [PubMed: 4191353]
9. Smith R, Francis MJO, Bauze RJ. Osteogenesis Imperfecta. Quaterly Journal of Medicine, New Series XLIV. 1975; 176:555–573.
10. Stacey A, Bateman J, Choi T, Mascara T, Cole W, Jaenisch R. Perinatal lethal osteogenesis imperfecta in transgenic mice bearing an engineered mutant pro-alpha 1(I) collagen gene. Nature. 1988; 332(6160):131–136. [PubMed: 2450280]
11. Bonadio J, Saunders TL, Tsai E, Goldstein SA, Morris-Wiman J, Brinkley L, Dolan DF, Altschuler RA, Hawkins JE Jr, Bateman JF, et al. Transgenic mouse model of the mild dominant form of osteogenesis imperfecta. Proc Natl Acad Sci U S A. 1990; 87(18):7145–7149. [PubMed: 2402497]
12. Hansen B, Jemec GB. The mechanical properties of skin in osteogenesis imperfecta. Arch Dermatol. 2002; 138(7):909–911. [PubMed: 12071818]
13. Ablin DS. Osteogenesis imperfecta: a review. Can Assoc Radiol J. 1998; 49(2):110–123. [PubMed: 9561014]
14. Bonadio J, Holbrook KA, Gelinas RE, Jacob J, Byers PH. Altered triple helical structure of type I procollagen in lethal perinatal osteogenesis imperfecta. J Biol Chem. 1985; 260(3):1734–1742. [PubMed: 2981871]
15. Steiner RD, Pepin M, Byers PH. Studies of collagen synthesis and structure in the differentiation of child abuse from osteogenesis imperfecta. J Pediatr. 1996; 128(4):542–547. [PubMed: 8618190]
16. Chevrel G, Meunier PJ. Osteogenesis imperfecta: lifelong management is imperative and feasible. Joint Bone Spine. 2001; 68(2):125–129. [PubMed: 11324928]
17. Glorieux FH. Experience with bisphosphonates in osteogenesis imperfecta. Pediatrics. 2007; 119:S163–S165. Suppl 2. [PubMed: 17332237]
18. Dent JA, Paterson CR. Fractures in early childhood: osteogenesis imperfecta or child abuse? J Pediatr Orthop. 1991; 11(2):184–186. [PubMed: 2010517]
19. Lund AM, Skovby F, Knudsen FU. Child abuse and osteogenesis imperfecta. How do we distinguish? Ugeskr Laeger. 2000; 162(11):1528–1533. [PubMed: 10868105]
20. Paterson CR, Burns J, McAllion SJ. Osteogenesis imperfecta: the distinction from child abuse and the recognition of a variant form. Am J Med Genet. 1993; 45(2):187–192. [PubMed: 8456801]
21. Chipman SD, Sweet HO, McBride DJ Jr, Davisson MT, Marks SC Jr, Shuldiner AR, Wenstrup RJ, Rowe DW, Shapiro JR. Defective pro alpha 2(I) collagen synthesis in a recessive mutation in mice: a model of human osteogenesis imperfecta. Proc Natl Acad Sci U S A. 1993; 90(5):1701–1705. [PubMed: 8446583]
22. Nicholls AC, Osse G, Schloon HG, Lenard HG, Deak S, Myers JC, Prockop DJ, Weigel WR, Fryer P, Pope FM. The clinical features of homozygous alpha 2(I) collagen deficient osteogenesis imperfecta. J Med Genet. 1984; 21(4):257–262. [PubMed: 6492090]
23. Camacho NP, Hou L, Toledano TR, Ilg WA, Brayton CF, Raggio CL, Root L, Boskey AL. The material basis for reduced mechanical properties in oim mice bones. J Bone Miner Res. 1999; 14(2):264–272. [PubMed: 9933481]
24. Saban J, Zussman MA, Havey R, Patwardhan AG, Schneider GB, King D. Heterozygous oim mice exhibit a mild form of osteogenesis imperfecta. Bone. 1996; 19(6):575–579. [PubMed: 8968022]
25. Ablett S, Burdett NG, Carpenter TA, Hall LD, Salter DC. Short echo time MRI enables visualisation of the natural state of human stratum corneum water in vivo. Magn Reson Imaging. 1996; 14(4):357–360. [PubMed: 8782172]
26. Bittoun J, Saint-Jalmes H, Querleux BG, Darrasse L, Jolivet O, Idy-Peretti I, Wartski M, Richard SB, Leveque JL. In vivo high-resolution MR imaging of the skin in a whole-body system at 1.5 T. Radiology. 1990; 176(2):457–460. [PubMed: 2367660]
27. Idy-Peretti I, Bittoun J, Alliot FA, Richard SB, Querleux BG, Cluzan RV. Lymphedematous skin and subcutis: in vivo high resolution magnetic resonance imaging evaluation. J Invest Dermatol. 1998; 110(5):782–787. [PubMed: 9579546]
28. Mirrashed F, Vennart W, Collier P, Summers IR. MRI characterisation of skin by MTC microimaging: correlation with skin function. Proc Intl SOc Magn Reson Med. 1999; 7:2130.

29. Richard S, Querleux B, Bittoun J, Idy-Peretti I, Jolivet O, Cermakova E, Leveque JL. In vivo proton relaxation times analysis of the skin layers by magnetic resonance imaging. J Invest Dermatol. 1991; 97(1):120–125. [PubMed: 2056181]
30. Richard S, Querleux B, Bittoun J, Jolivet O, Idy-Peretti I, de Lacharriere O, Leveque JL. Characterization of the skin in vivo by high resolution magnetic resonance imaging: water behavior and age-related effects. J Invest Dermatol. 1993; 100(5):705–709. [PubMed: 8388010]
31. Song HK, Wehrli FW, Ma J. In vivo MR microscopy of the human skin. Magn Reson Med. 1997; 37(2):185–191. [PubMed: 9001141]
32. Weis J, Ericsson A, Hemmingsson A. Chemical shift artifact-free microscopy: spectroscopic microimaging of the human skin. Magn Reson Med. 1999; 41(5):904–908. [PubMed: 10332872]
33. Zemtsov A, Lorig R, Ng TC, Xue M, Bailin PL, Bergfeld WF, Larson K, Yetman R. Magnetic resonance imaging of cutaneous neoplasms: clinicopathologic correlation. J Dermatol Surg Oncol. 1991; 17(5):416–422. [PubMed: 2030203]
34. Sharma R. Microimaging of hairless rat skin by magnetic resonance at 900 MHz. Magn Reson Imaging. 2008
35. Chen CT, Fishbein KW, Torzilli PA, Hilger A, Spencer RG, Horton WE Jr. Matrix fixed-charge density as determined by magnetic resonance microscopy of bioreactor-derived hyaline cartilage correlates with biochemical and biomechanical properties. Arthritis Rheum. 2003; 48(4):1047–1056. [PubMed: 12687548]
36. Laurent D, Wasvary J, Yin J, Rudin M, Pellas TC, O'Byrne E. Quantitative and qualitative assessment of articular cartilage in the goat knee with magnetization transfer imaging. Magn Reson Imaging. 2001; 19(10):1279–1286. [PubMed: 11804755]
37. Fragonas E, Mlynarik V, Jellus V, Micali F, Piras A, Toffanin R, Rizzo R, Vittur F. Correlation between biochemical composition and magnetic resonance appearance of articular cartilage. Osteoarthritis Cartilage. 1998; 6(1):24–32. [PubMed: 9616436]
38. Seo GS, Aoki J, Moriya H, Karakida O, Sone S, Hidaka H, Katsuyama T. Hyaline cartilage: in vivo and in vitro assessment with magnetization transfer imaging. Radiology. 1996; 201(2):525–530. [PubMed: 8888253]
39. Mosher TJ, Liu Y, Yang QX, Yao J, Smith R, Dardzinski BJ, Smith MB. Age dependency of cartilage magnetic resonance imaging T2 relaxation times in asymptomatic women. Arthritis Rheum. 2004; 50(9):2820–2828. [PubMed: 15457450]
40. Laurent D, Wasvary J, O'Byrne E, Rudin M. In vivo qualitative assessments of articular cartilage in the rabbit knee with high-resolution MRI at 3 T. Magn Reson Med. 2003; 50(3):541–549. [PubMed: 12939762]
41. Laurent D, Wasvary J, Rudin M, O'Byrne E, Pellas T. In vivo assessment of macromolecular content in articular cartilage of the goat knee. Magn Reson Med. 2003; 49(6):1037–1046. [PubMed: 12768582]
42. Sims TJ, Miles CA, Bailey AJ, Camacho NP. Properties of collagen in OIM mouse tissues. Connect Tissue Res. 2003; 44:202–205. Suppl 1. [PubMed: 12952198]
43. West P, Torzilli PA, Chen C, Lin P, Camacho NP. Fourier tranform infrared imaging spectroscopy analysis of collagenase-induced cartilage degradation. Journal of Biomed Opt. 2005; 10(1):14015.
44. Faibish D, Gomes A, Boivin G, Binderman I, Boskey A. Infrared imaging of calcified tissue in bone biopsies from adults with osteomalacia. Bone. 2005; 36(1):6–12. [PubMed: 15663997]
45. Kocher MS, Shapiro F. Osteogenesis imperfecta. J Am Acad Orthop Surg. 1998; 6(4):225–236. [PubMed: 9682085]
46. Holbrook KA, Byers PH. Structural abnormalities in the dermal collagen and elastic matrix from the skin of patients with inherited connective tissue disorders. J Invest Dermatol. 1982; 79:7s–16s. Suppl 1. [PubMed: 6806400]
47. Laurent S, Elst LV, Copoix F, Muller RN. Stability of MRI paramagnetic contrast media: a proton relaxometric protocol for transmetallation assessment. Invest Radiol. 2001; 36(2):115–122. [PubMed: 11224760]
48. Potter K, Butler JJ, Horton WE, Spencer RG. Response of engineered cartilage tissue to biochemical agents as studied by proton magnetic resonance microscopy. Arthritis Rheum. 2000; 43(7):1580–1590. [PubMed: 10902763]

49. Renou JP, Bonnet M, Bielicki G, Rochdi A, Gatellier P. NMR study of collagen-water interactions. Biopolymers. 1994; 34(12):1615–1626. [PubMed: 7849224]
50. Fishbein KW, Gluzband YA, Kaku M, Ambia-Sobhan H, Shapses SA, Yamauchi M, Spencer RG. Effects of formalin fixation and collagen cross-linking on T2 and magnetization transfer in bovine nasal cartilage. Magn Reson Med. 2007; 57(6):1000–1011. [PubMed: 17534923]
51. Francis MJ, Smith R, Bauze RJ. Instability of polymeric skin collagen in osteogenesis imperfecta. Br Med J. 1974; 1(5905):421–424. [PubMed: 4816854]
52. Mirrashed F, Sharp JC. In vivo morphological characterisation of skin by MRI micro-imaging methods. Skin Research and Technology. 2004; 10:149–160. [PubMed: 15225264]
53. Bittoun J, Querleux B, Darrasse L. Advances in MR imaging of the skin. NMR Biomed. 2006; 19(7):723–730. [PubMed: 17075954]
54. Lusse S, Claassen H, Gehrke T, Hassenpflug J, Schunke M, Heller M, Gluer CC. Evaluation of water content by spatially resolved transverse relaxation times of human articular cartilage. Magn Reson Imaging. 2000; 18(4):423–430. [PubMed: 10788720]
55. Knauss R, Fleischer G, Grunder W, Karger J, Werner A. Pulsed field gradient NMR and nuclear magnetic relaxation studies of water mobility in hydrated collagen II. Magn Reson Med. 1996; 36(2):241–248. [PubMed: 8843378]
56. Nieminen MT, Toyras J, Rieppo J, Hakumaki JM, Silvennoinen J, Helminen HJ, Jurvelin JS. Quantitative MR microscopy of enzymatically degraded articular cartilage. Magn Reson Med. 2000; 43(5):676–681. [PubMed: 10800032]
57. Traore A, Foucat L, Renou JP. 1H-nmr study of water dynamics in hydrated collagen: transverse relaxation-time and diffusion analysis. Biopolymers. 2000; 53(6):476–483. [PubMed: 10775063]
58. Reiter DA, Lin PC, Fishbein KW, Spencer RG. Multicomponent T2 relaxation analysis in cartilage. Magn Reson Med. 2009; 61(4):803–809. [PubMed: 19189393]
59. Yamamoto K, Yamauchi M. Characterization of dermal type I collagen of C3H mouse at different stages of the hair cycle. Br J Dermatol. 1999; 141(4):667–675. [PubMed: 10583114]
60. McBride DJ Jr, Choe V, Shapiro JR, Brodsky B. Altered collagen structure in mouse tail tendon lacking the alpha 2(I) chain. J Mol Biol. 1997; 270(2):275–284. [PubMed: 9236128]
61. Bi X, Yang X, Bostrom MP, Bartusik D, Ramaswamy S, Fishbein KW, Spencer RG, Camacho NP. Fourier transform infrared imaging and MR microscopy studies detect compositional and structural changes in cartilage in a rabbit model of osteoarthritis. Anal Bioanal Chem. 2007; 387(5):1601–1612. [PubMed: 17143596]
62. Potter K, Butler JJ, Adams C, Fishbein KW, McFarland EW, Horton WE, Spencer RG. Cartilage formation in a hollow fiber bioreactor studied by proton magnetic resonance microscopy. Matrix Biol. 1998; 17(7):513–523. [PubMed: 9881603]
63. Kim M, Bi X, Horton WE, Spencer RG, Camacho NP. Fourier transform infrared imaging spectroscopic analysis of tissue engineered cartilage: histologic and biochemical correlations. J Biomed Opt. 2005; 10(3):031105. [PubMed: 16229630]
64. Pedersen L, Hansen B, Jemec GB. Mechanical properties of the skin: a comparison between two suction cup methods. Skin Res Technol. 2003; 9(2):111–115. [PubMed: 12709128]
65. Gajko-Galicka A. Mutations in type I collagen genes resulting in osteogenesis imperfecta in humans. Acta Biochim Pol. 2002; 49(2):433–441. [PubMed: 12362985]

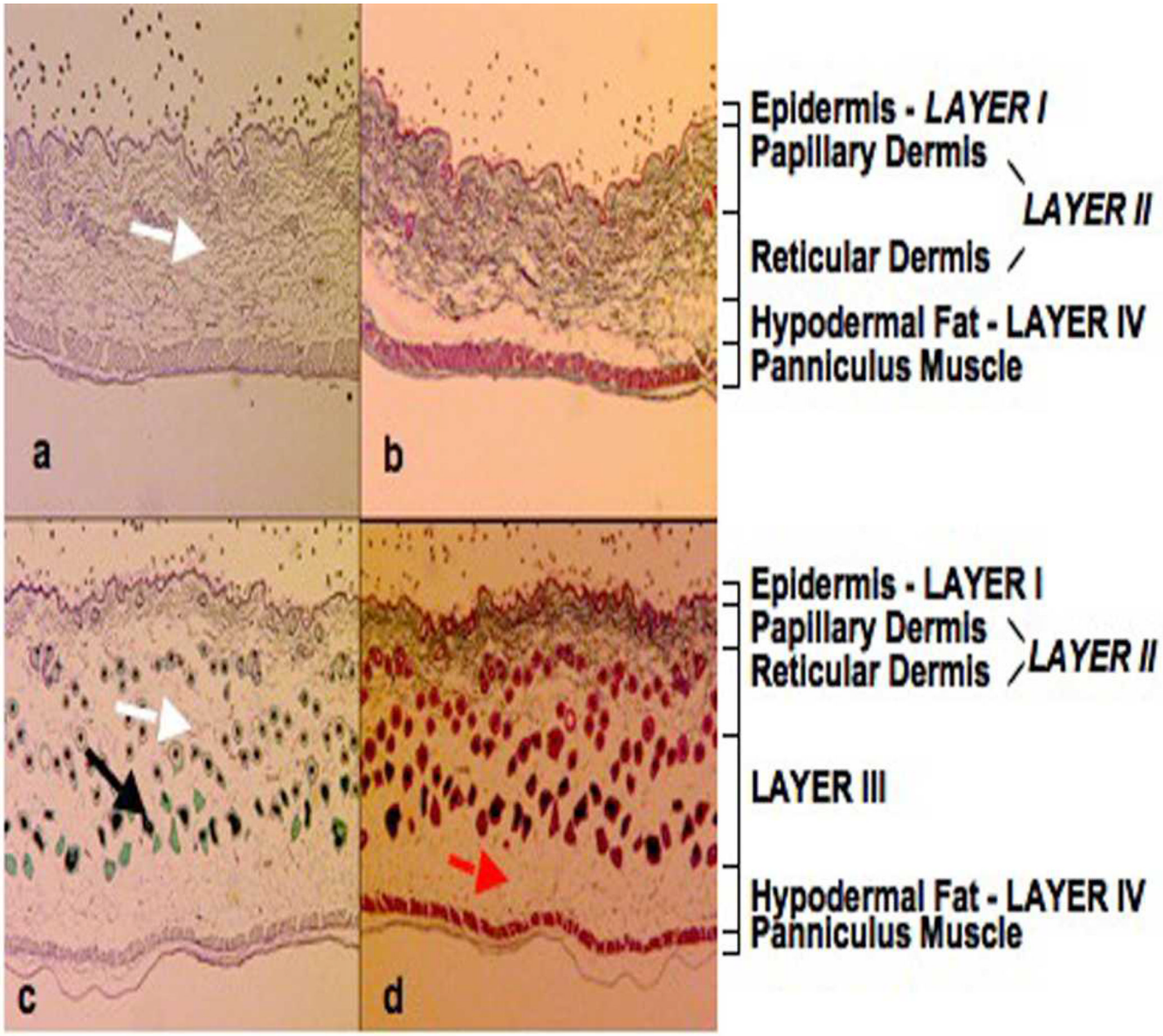

Figure 1.

Luna (**a** and **c**) Masson's trichrome (**b** and **d**) histological staining of mouse skin from the dorsum of wildtype (+/+) and homozygous *oim/oim* mice. The Masson's trichrome stain demonstrated a much reduced region of collagen-rich tissue in the *oim/oim* compared to the +/+ animals and an increase in dermal adipose tissue (red arrow). The Luna stain showed a loss of elastin fibers (white arrow) in the lower reticular dermal layer (lower part of layer II and layer III) of the *oim/oim* compared to the +/+ skin samples. In the *oim/oim* mouse many hair follicles were present that were in the anagen stage of hair growth, with large, heavily pigmented, melanin-rich, hair bulbs. The hair follicles (black arrow) had thick root sheaths, while sebaceous glands were small and inconspicuous. Epidermis – Layer I, Papillary Dermis and Reticular Dermis – Layer II and Hypodermal Fat – Layer IV.

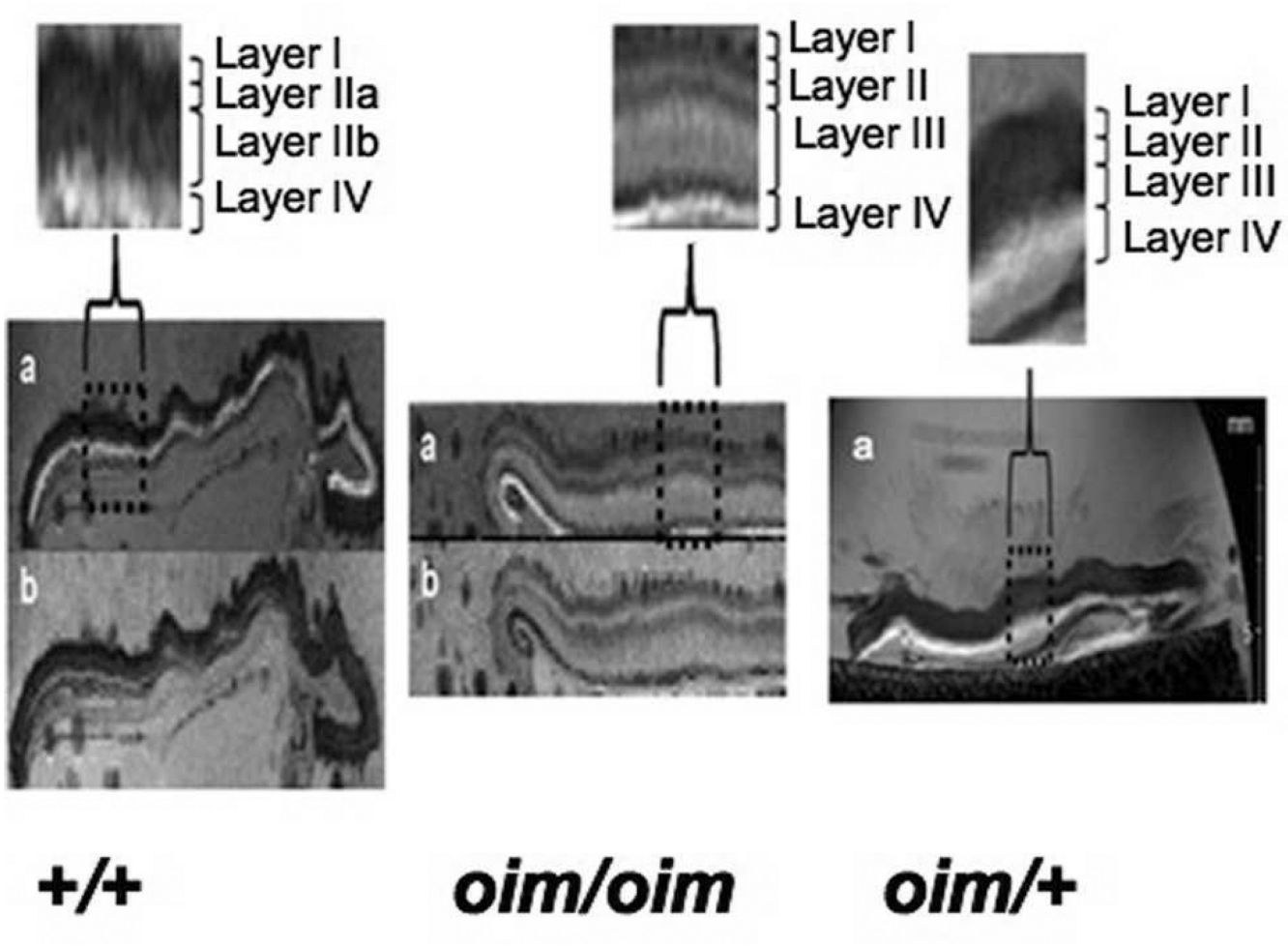

Figure 2.

T_2-weighted images (a) showed a clear demarcation of individual skin layers in the wildtype control (+/+) and homozygous (*oim/oim*) mice skin samples. The fat suppression techniques (TE = 12 ms, TR = 15 s, NEX= 2) caused the hypodermal fat layer to be darkened (b) thus permitting the identification of any fatty layers in the MR image. Differentiation of the reticular dermal layer into an upper (layer II) and a lower layer (layer III) was seen in all the *oim/oim* skin samples, and in one out of the four heterozygous (*oim/+*) skin samples examined (pictured). Layers lla and llb correspond to the papillary and reticular dermis, respectively.

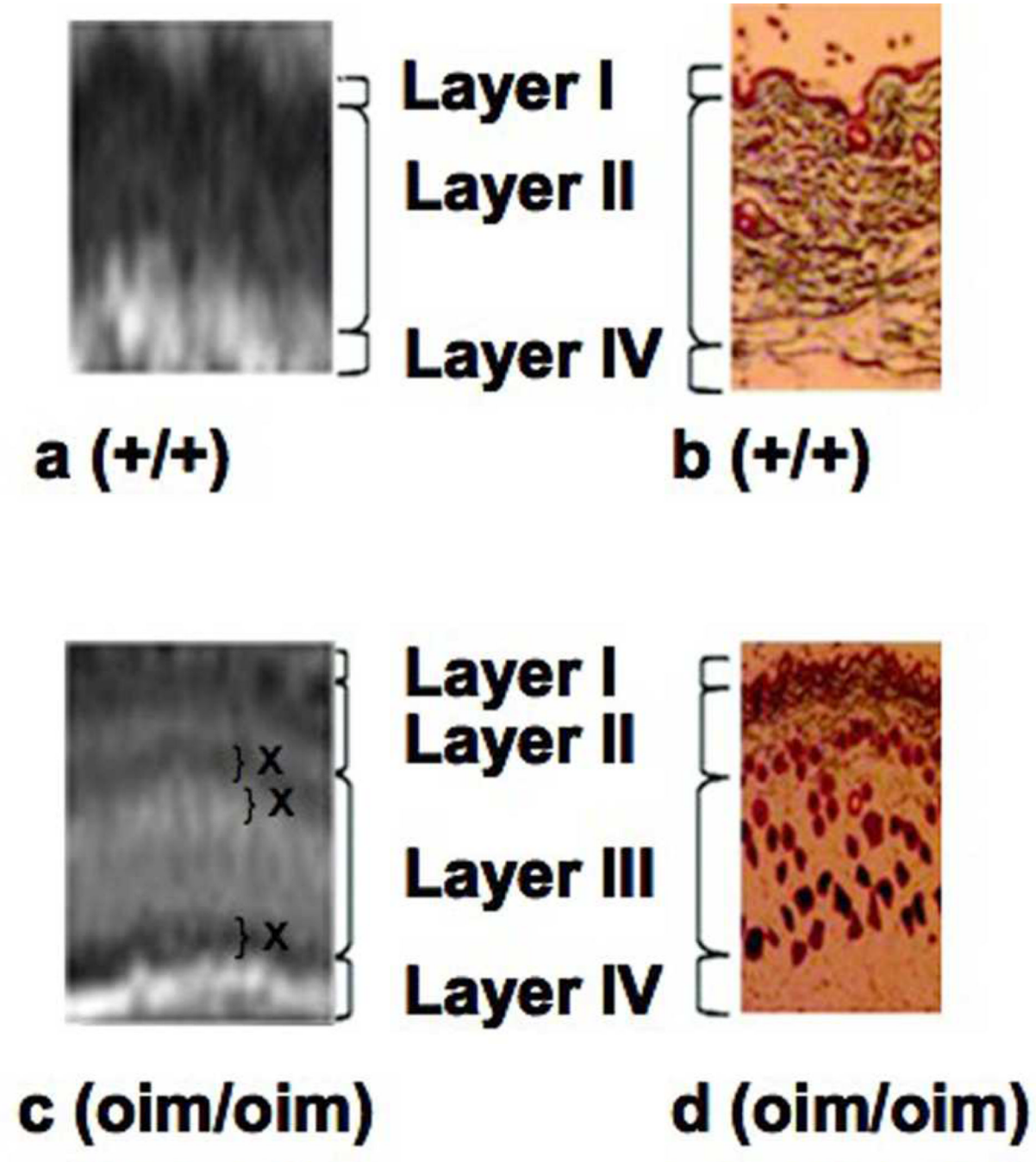

Figure 3.
Comparison of MR T_2-weighted images and Masson's trichrome staining for collagen show a correspondence between the layers observed using the two techniques. Horizontal contrast banding (marked with an X in layers II and III) is an indication of the lack of homogeneous hydration across these layers in the *oim/oim* samples.

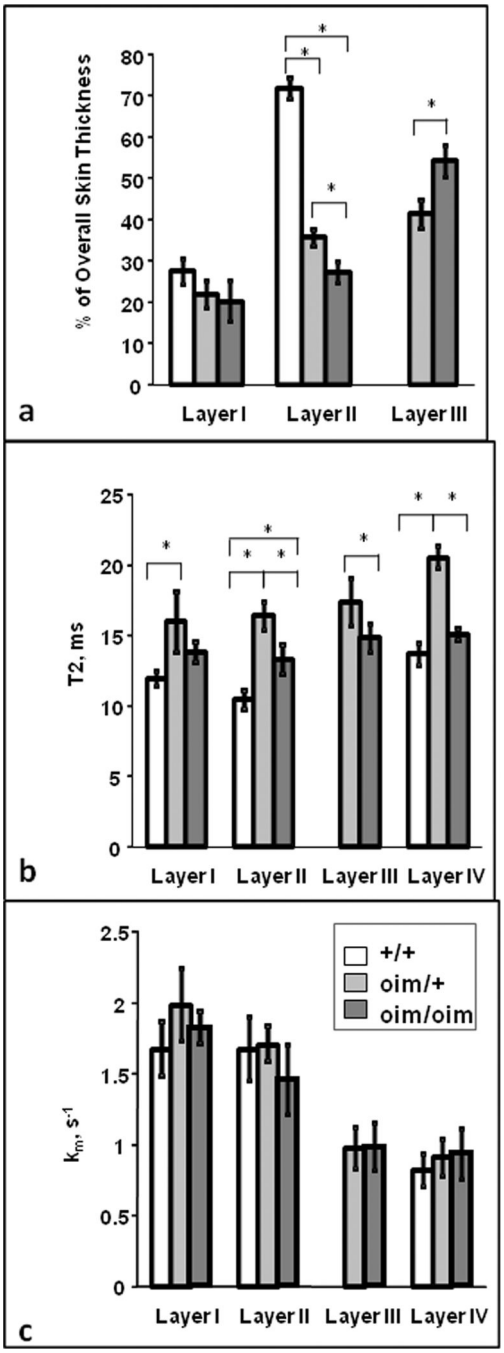

Figure 4.

Comparison of MRI-determined thickness and biophysical parameters among genotypes in individual layers, where layer I = epidermis, layer II = papillary and reticular dermis, layer III = extended lower dermal layer in oim genotypes, and layer IV = fat layer. (* $p < 0.05$ between genotypes). **a)** Individual skin layer thickness, measured as a % of the total skin layer. There was no difference in thickness of layer I among genotypes. Layer II was significantly reduced in the *oim*/+_and *oim/oim* mice compared to the +/+ mice, and in the *oim/oim* compared to the *oim*/+ mice. Layer III was significantly thicker in the *oim/oim* mice compared to the *oim*/+ mice. **b)** The highest T_2 values for all genotypes were seen in the

hypodermal fat layer IV. T_2 values for the *oim*/+_mice were significantly higher than those for the +/+ in layers I, II and IV, and significantly higher than those for the *oim/oim* in layers II, III and IV. Further, the *oim/oim* values were significantly higher than the +/+ values in layers II and IV. **c)** There were no significant differences in measured k_{MT} ($s^{\#x02212;1}$) values among the three genotypes within each layer.

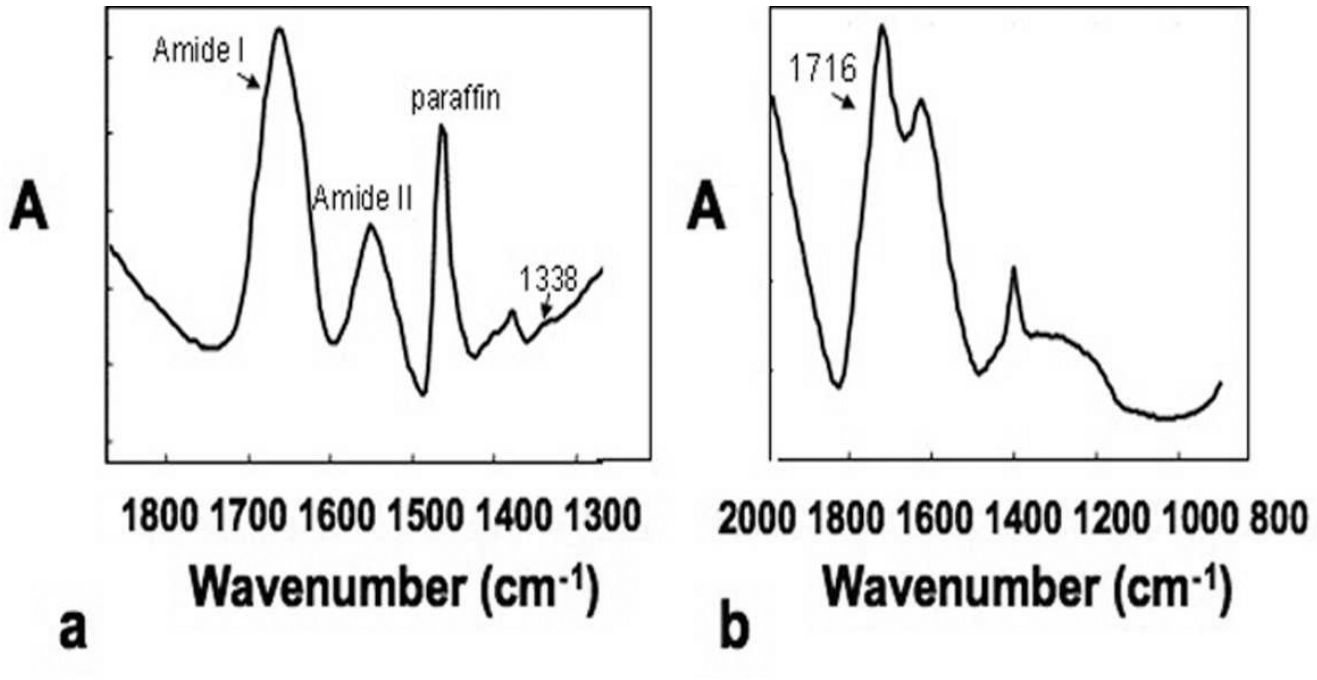

Figure 5.

a) Infrared spectrum obtained from the dermal layer of a wildtype mouse skin. Absorbances (A) specific to collagen are the amide I (C=O stretching vibration), amide II (C-N stretch and N-H bend combination vibration) and the 1338 $cm^{\#x02212;1}$, an absorbance that arises from amino acid sidechain rotations. **b)** Infrared spectrum of pure melanin powder. The 1716 $cm^{\#x02212;1}$ absorbance was utilized to map the distribution of melanin in the skin sections.

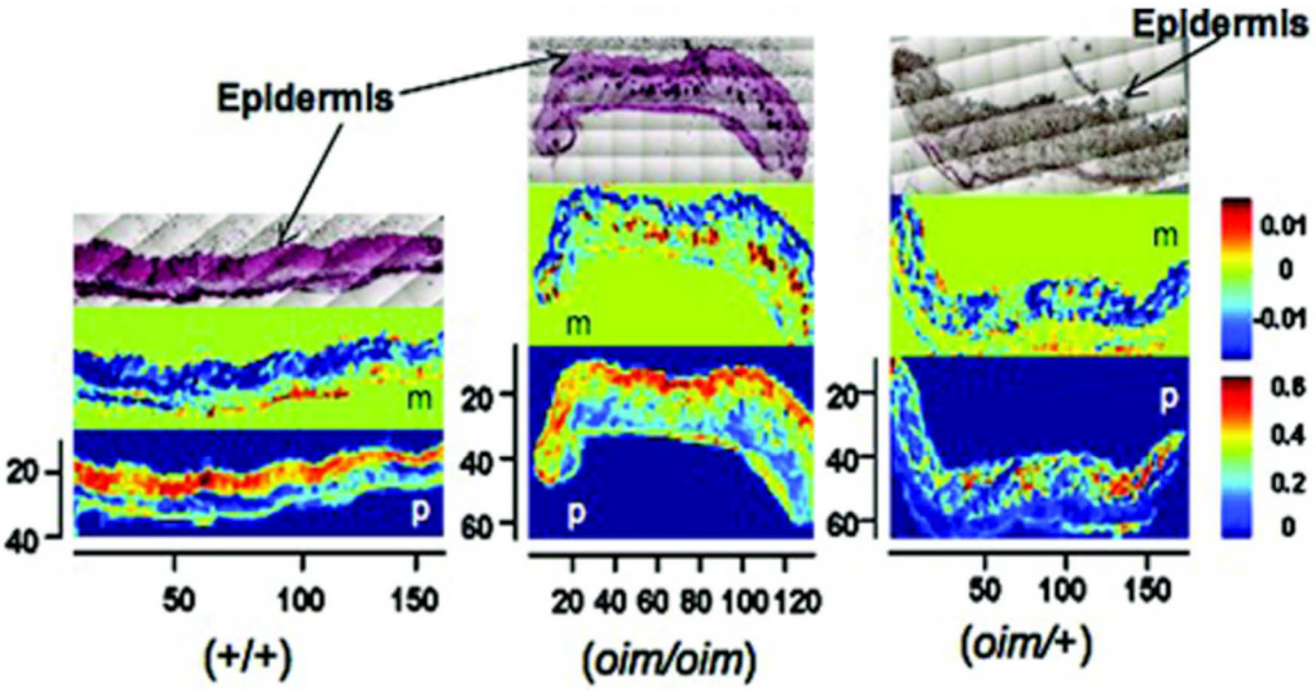

Figure 6.

H&E stained histology images (top row) and the corresponding FT-IRIS images of melanin distribution (middle row, marked “m”) and protein distribution (bottom row, marked ‘p’) for +/+, *oim/oim* and *oim*/+ animals. The pixilation seen on the histology slides allows for reproducible magnification and orientation in the FT-IRlS microscope. The axes shown are in pixels, where 1 pixel = 25 microns. The units of the color bars are integrated area of absorbance. The *oim/oim* tissues showed a strong correspondence between the dark, spotted regions in the fatty layer of the HE stained sections and the high concentration and distribution of melanin in the FT-IRIS image. The protein distribution showed a higher concentration in the dermal regions compared to the fatty layer for all samples, reflecting the presence of collagen.

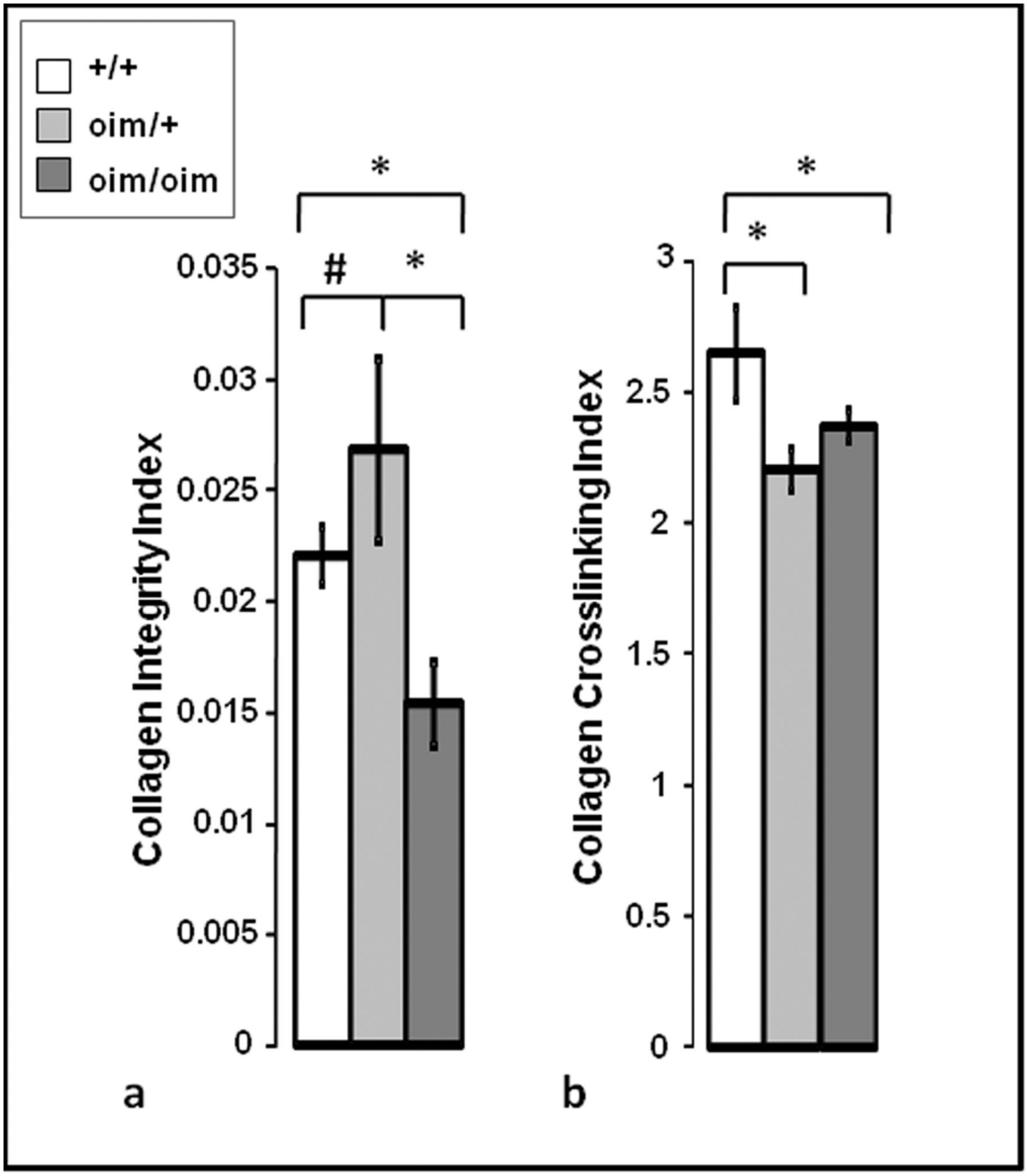

Figure 7.

a) The collagen integrity parameter (calculated from the ratio of the integrated area under the infrared 1338 peak (1356–1324 $cm^{\#x02212;1}$) to the area under the amide II peak (1588–1488 $cm^{\#x02212;1}$)) was found to be significantly lower in the *oim/oim* tissues compared to both the +/+ and *oim*/+ tissues (*$p < 0.05$). There was a trend (#$p = 0.07$) towards higher values in the *oim*/+ compared to the +/+ tissues. **b)** The collagen crosslink parameter was calculated as the ratio of the peak heights at 1660 $cm^{\#x02212;1}$ and 1690 $cm^{\#x02212;1}$ and was found to be significantly lower in the *oim/oim* and +/*oim* tissues compared to the +/+ tissues (* $p < 0.05$).